# Anti-Ohmic Nanoconductors: Myth, Reality and Promise

Ashima Bajaj and Md. Ehesan Ali*

*Institute of Nano Science and Technology, Sector-81, Mohali, Punjab-140306, India*

E-mail: ehesan.ali@inst.ac.in

**Abstract**

The recent accomplishment in the design of molecular nanowires characterized by an increasing conductance with length have embarked the origin of extraordinary new family of molecular junctions referred to as "anti-ohmic" wires. Herein, this highly desirable, non-classical behavior, has been examined for the longer enough molecules exhibiting pronounced diradical character in their ground state within the unrestricted DFT formalism with spin and spatial symmetry breaking. We demonstrate that highly conjugated acenes signal higher resistance in open-shell singlet (OSS) configuration as compared to their closed-shell counterparts. This anomaly has been further put to proof for experimentally certified cumulene wires, which reveals phenomenal modulation in the transport characteristics such that an increasing conductance is observed in closed-shell limit, while higher cumulenes in OSS ground state yield a regular decay of conductance.

## 1 Introduction

Molecular nanowires mediating long range charge transport are desirable for their potential applications in future molecular scale circuitry.[1–3] Most of the conventional molecular wires

suffer from an exponential decay of conductance (G) with wire length (L) as $G = Ae^{-\beta L}$, wherein positive $\beta$ value signifies a decay of conductance. However, in recent years, molecular wires with unusual attenuation factors, such as $\beta$=0 (i.e., G independent of L)[4] or even negative $\beta$ values (i.e., G increasing with L) have become sparkle in the eyes of research community.[5–7] Such extraordinary wires exhibiting negative $\beta$ values in phenomenological violation of the classical Ohm's law are called as anti-ohmic nanoconductors. This reversed exponential decay of conductance with length was first reported by Tada and Yoshizawa for nanographenes with zigzag edges.[8] Subsequently, the molecular wires based on porphyrin derivatives were presented with low attenuation factors[9,10] which was later endorsed by an experimental achievement by Leary et al.[11] Afterwards, several guiding principles were formulated to explain the non-trivial reversed conductance/length trends. Tsuji et al. suggested that if the bond length alternation of molecule is reversed, $\beta$ will be negative.[12] Mandado and coworkers proposed an example of quinoid wires with exceptional anti-ohmic behavior.[13] Other correlated factors including captodative substitution and effect of aromaticity have also been employed to enhance conductivity.[14,15]

Another commonly employed method to achieve the reverse conductance-length trend is to design wires with diradical character, following the SSH model for 1D topological insulators.[6,16] The concept of diradical character is associated with the open-shell nature of polycyclic aromatic hydrocarbons (PAHs) and is qualitatively understood by the increasing contribution of open shell resonance forms to the ground state electronic structure. An argument relating the transmission probability to the weight of diradical resonance structures in the resonance hybrid of the molecule was also given by Hoffmann et al.[17] Accordingly, the diradicals can have large transmission around the Fermi energy if and only if the positions of contacts to the electrodes are chosen on carbon atoms on which radical centers can localize. Alongside, using restricted DFT based methods, Stuyver et al. connected the anti-ohmic behavior to the increasing diradical character.[18] Contrastingly, in the framework of multi-reference calculations, Mandado et al. observed a regular decay of conductance.[19] Followed

by this, unrestricted DFT calculations taking into account the spin-symmetry breaking also revealed a decrease in conductance with length for the alleged anti-ohmic wires.[20] Thus, putting a question mark over the relation between diradical character and conductance.

With these ongoing trial and error debates on the feasibility of anti-ohmic wires, we undertook a theoretical investigation of length-dependence of the conductance in molecular wires exhibiting pronounced diradical character in their ground state. In the context of diradical character, the highly conjugated polyacenes, consisting of linearly fused benzene rings, have been widely debated in literature.[21,22] Using unrestricted B3LYP calculations, Bendikov et al. established that smaller acenes (up to hexacene) have a closed-shell singlet (CSS) ground state, while higher acenes are predicted to be in open-shell singlet (OSS) ground state. This OSS state was found to be diradical in nature, consisting of two singly occupied molecular orbitals (SOMOs), each one localized on one of the two long edges with an anti-ferromagnetic coupling of unpaired electrons localized on the opposite edges.[23] Afterwards, numerous experimental[24,25] and theoretical[26–31] reports aimed to validate the OSS ground state of higher order polyacenes. Employing a density matrix renormalization group (DMRG) algorithm by performing a full $\pi$-valence space CASSCF calculations, Chan et al. reached the same conclusion with OSS ground state for higher acenes (n >7).[26] Followed by this, Jiang et al. also establised OSS ground state (n >7) based on spin-polarized generalized gradient approximation (GGA) calculations.[27] However, the later two studies claimed that higher acenes (beyond n =12) are polyradical in nature, with more than one unpaired electrons accumulating on each of the edge. Indeed the corresponding natural orbital (NO) occupation numbers also turned out to be fractional, not only for the frontier highest occupied natural orbital (HONO) and lowest unoccupied natural orbital (LUNO), but also for the next nearest orbitals, i.e., HONO-1 and LUNO+1. Lately, particle–particle random-phase approximation (pp-RPA) calculations by Yang et al. gave the same qualitative answer, however, pushing the CSS to OSS crossover to larger acenes from n = 10 onwards.[29] By means of Quantum Monte Carlo (QMC) methods, Dupuy et al. also found that the

polyacenes exhibit a weak diradical character at least until n = 9.[30] Using symmetry-broken DFT methods, Malrieu et al. demonstrated the evolution of OSS state from n =7 onwards, while the appearance of second spin symmetry breaking for n = 13 with four unpaired electrons centered at edges, thus presenting a simple picture compatible with the conclusions of best computations.[31] In nutshell, different quantum chemistry methods used till date to understand the electronic structure of polyacenes have demonstrated different threshold length at which the CSS to OSS conversion takes place, however all of them agree to the same qualitative picture with open-shell diradical or polyradical character which increases progressively with the increasing length of polyacene series.

Proceeding towards the conductance calculations, the transport characteristics of acenes with increasing length have been examined by numerous theoretical reports,[32–36] while the effect of spin polarized nature of higher acenes on the electron transport has been rarely considered.[37] Assuming the non-magnetic ground state, Visontai et al. found that conductance of the acene series is an oscillatory function of length due to quantum interference (QI) effects.[38] In an experimental study, Kaliginedi et al. observed an exponential decay of conductance for lower acenes with positive $\beta$ value.[39] While a recent computational study by valdiviezo et al. claimed that acenes with meta connection to electrodes exhibits reversed exponential decay of conductance with length.[40] Thus, the length dependence of conductance for acenes has remained a persistent puzzle.

On the other hand, poles apart from polyacenes, there had been many speculations about 1-D linear chain of sp-hybridized carbon atoms, which potentially exist in two forms: polyynes with alternate single and triple bonds and cumulenes with consecutive double bonds.[41,42] Among the two series, cumulenes have seen the light of the day with an experimental observation of negative $\beta$ values.[43,44] Notwithstanding, the synthesis of polyynes has been extensively reported, culminating with the isolation of [22]polyyne, however, due to dramatic increase in reactivity, [9]cumulene is the longest derivative studied to date.[45,46] This increased reactivity of [$n$]cumulenes itself points towards the open-shell character in

longer cumulenes. However, the open-shell nature of cumulenes has not been reported hitherto. Here, in this work, we sought to re-examine the contradictory length dependence of molecular conductance for the acene series suspended between two gold electrodes. To further simulate the experimentally validated anti-ohmic behaviour in cumulene wires,[43] phenyl substituted cumulene wires are chosen. The electrical conductance has been explicitly determined within the Landauer formalism using restricted closed-shell wavefunction for lower members in the series. While, broken symmetry (BS) wavefunction in an unrestricted formalism with spin and spatial symmetry breaking is used for higher members with OSS ground state.

## 2 Computational Methodology

Geometry optimization of isolated dithiolated molecules are first performed by applying B3LYP/def2-TZVP[47,48] method in two distinct electronic states, i.e., closed shell singlet (CSS) and broken symmetry open shell singlet (OSS) state in ORCA[49] quantum chemical code. OSS states are treated using spin-unrestricted broken-symmetry Kohn-Sham (UKS-BS) method within the DFT framework, while spin-restricted (RKS) wavefunction is used for CSS states. Resolution of the identity (RI) approximation in conjunction with auxiliary basis set def2/J and chain of spheres (COSX) numerical integration is used to accelerate the calculations without losing its accuracy.[50] Tight convergence limits and increased integration grids (grid5) are used throughout. The molecular junctions are then constructed by placing the optimized isolated dithiol molecules between two gold electrodes after removing the terminal hydrogen atoms of thiol groups and forming the S-Au bonds. The gold electrodes are approximated by nine-atomic gold clusters, arranged in hexagonal closed-packed fcc Au-111 surface. The Au-Au distance is set to 2.88 Å and Au-S distance is fixed to 2.40 Å, which is similar to our previous reported works.[51,52]

The electron transport calculations are performed using Non-Equilibrium Green's Func-

tion combined with DFT (NEGF-DFT) as implemented in *Artaios*[53] using B3LYP exchange correlation functional in combination with LANL2DZ basis set. Accordingly, the model used in transmission calculations is divided into three regions: central (C) scattering region formed by the di-thiolated molecule, and the left (L) and right (R) electrode consisting of $Au_9$ clusters. The transmission function is computed in the spirit of Landauer-Büttiker[54] formalism using equation

$$T_\sigma(E) = Tr(\Gamma_R G \Gamma_L G^\dagger)_\sigma \tag{1}$$

where $\sigma$ represents the spin up/down electrons. $G/G^\dagger$ indicates the retarted/advanced Green's function of the central region. The coupling of central region to the electrodes is taken into account using self-energies, which are calculated by imposing a wide-band limit approximation[55] which assumes a constant density of states, independent of energy. A constant value of 0.036 $ev^{-1}$, taken from literature is used for the DOS of electrode.[56]

The zero bias conductance in CSS limit is obtained as

$$G = \frac{2e^2}{h} T(E_F) \tag{2}$$

For spin-polarized systems in OSS state, transmission for spin-up ($T_{up}$) and spin-down ($T_{down}$) are different, therefore, the conductance in OSS state at Fermi energy is computed as

$$G = \frac{e^2}{h}(T_{up}(E_F) + T_{down}(E_F)) \tag{3}$$

It is worth mentioning that while B3LYP functional is routinely employed for conductance calculations, however it tends to underestimate the HOMO-LUMO gap as compared to the fundamental gap (calculated as difference between ionization potential and electron affinity).[57] This is reflected in the form of overestimated conductance (by about 1-2 orders of magnitude) as compared to the experimental values. This limitation can be addressed by using a range-separated hybrid (RSH) functionals, which have been demonstrated to predict better HOMO-LUMO gaps[58] and provide realistic conductance estimates.[59,60] Interestingly,

the calculated conductance using CAM-B3LYP, an RSH functional (SI, Section 7) yields similar qualitative trends as of B3LYP with improved conductance values, but at the cost of severe spin contamination in OSS state.

# 3 Results and Discussions

## 3.1 Electronic structure of isolated molecules

While the CSS ground state for lower acenes and cumulenes is well recognized in literature, but there is no clear consensus on the higher members of the series, yet. Thus, to establish the size-dependent onset of open-shell nature, ground state electronic properties are first examined for the isolated acenes and cumulenes, shown in insets of Figure 1. The relative energy difference between the OSS and CSS states, reveals that upto $n$=6 acene (Figure 1a) and $n$=12 cumulene (Figure 1c), OSS solutions converge to CSS state and yields $\Delta E_{OSS-CSS}$ $\sim$ 0, indicating that CSS state is ground state for the lower members of both the series. For $n$=7 acene, $\Delta E_{OSS-CSS}$ = -65 meV marks the transition in ground state from CSS to OSS state. The increasing $\Delta$E upto -650 meV for $n$=12, ultimately outstrip the CSS behavior of the system for higher acenes. The emergence of OSS ground state, for n $\geq$ 7, is in complete agreement with previous DFT calculations on higher acenes.[23,31] Interestingly, the similar kind of build-up of OSS character is also observed for cumulenes from $n$=14 onwards (Figure 1c). Although, $\Delta E_{OSS-CSS}$ for cumulenes is significantly lower than acenes, however a maxima of $\Delta E_{OSS-CSS}$ = -138 meV for $n$=24 cumulene clearly reveals an OSS ground state for the higher cumulenes as well.

To further validate the OSS character, spin-squared value $<S^2>$ in BS state and radicaloid character ($y$), which are used as the descriptors of diradical character of a molecule[61,62] are presented in Figure 1b and Figure 1d. The diagnostic value of $<S^2>$ in BS determinant should be 1.0. Any deviation from the expected $<S^2>_{BS}$ =1 indicates spin contamination due to contributions from other low lying excited spin states. Here, $<S^2>$ =0 upto $n$=5

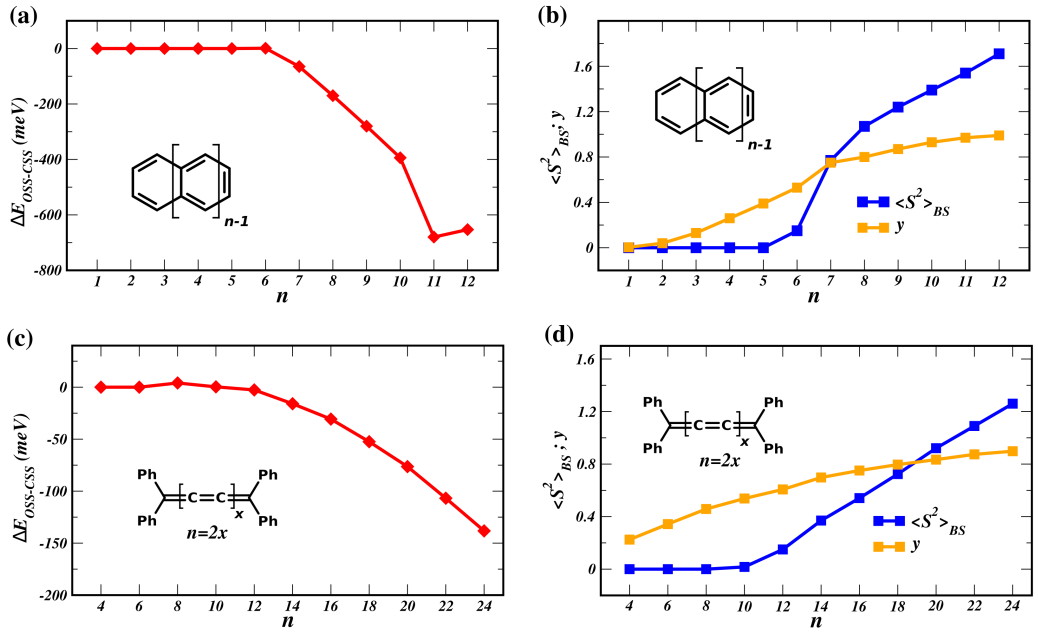


**Figure 1:** (a,c) Relative energy difference ($\Delta E_{OSS-CSS}$) in meV calculated at B3LYP/def2-TZVP level using unrestricted broken-symmetry DFT for OSS state and restricted DFT for CSS state for (a) $n = 1$ to 12 acenes, (c) $n = 4$ to 24 cumulenes. (b,d) Computed $<S^2>$ values in BS state at UB3LYP/def2-TZVP level and radicaloid character ($y$) for (b) acenes, (d) cumulenes, blue curve denotes variation in $<S^2>_{BS}$ values and orange curve represent $y$ values. The negative $\Delta E_{OSS-CSS}$, increasing $<S^2>$ and $y > 0.6$ indicates that OSS state is favoured as a ground state from $n = 7$ acene and $n = 14$ cumulene onwards.

acene and $n$=10 cumulene indicates CSS ground state. Afterwards, the $<S^2>$ value shows a regular increase with the increasing $n$ for both the series. For intermediate members, i.e., $n$=6 acene and $n$=12 cumulene, $<S^2>_{BS} \sim 0.17$ indicates the preferential existence of molecule in CSS ground state. Thereafter, $<S^2>_{BS}$ starts approaching towards 1.0 indicating diradical ground state for n $\geq$ 7 for acenes and n $\geq$ 14 for cumulenes. However, for the higher members, the spin contamination in OSS becomes large with $<S^2> = 1.69$ for $n$=12 acene and 1.26 for $n$=24 cumulene pointing towards the mixing of low-lying triplets. Qualitatively, similar trends are also found in radicaloid character ($y$), which classify singlet molecular systems into three categories: (i) closed- shell ($y = 0$), (ii) intermediate diradical ($0 < y < 1$), (iii) pure open-shell ($y = 1$) systems.[63] The increasing radicaloid character with increasing length, i.e., $y > 0.6$ from $n$=7 acene and $n$=14 cumulene onwards confirms that OSS spin polarized state supersedes the CSS state as the ground state (SI, Section 3).

## 3.2 Evolution of transport characteristics for Acenes

With such an understanding for the ground state electronic properties, we proceed to investigate the behavior of molecules with OSS ground state in molecular devices. To do so, acenes and cumulenes are placed between two gold electrodes consisting of two $Au_9$ clusters via thiol anchoring groups, as shown in Figure 2a and Figure 3a.

Before proceeding, let's make the discussion more concrete by focusing on the elemental factors that influence the conductance.[8] The argument embarks on the familiar zeroth order Green's function[64] derived in the Caroli-Combescot-Landauer (CCL) formulation employing Pariser-Parr-Pople (PPP) Hamiltonian[65] (not stemming from NEGF formulation) written as

$$G_{lr}^{mol}(E) = \frac{C_{l,HOMO}C^{\star}_{r,HOMO}}{E - \varepsilon_{HOMO}} + \frac{C_{l,LUMO}C^{\star}_{r,LUMO}}{E - \varepsilon_{LUMO}} \tag{4}$$

where $C_{l/r,HOMO}$ and $C_{l/r,LUMO}$ are the MO coefficients of the HOMO and LUMO at the connecting sites $l$ and $r$ and $\varepsilon_{HOMO/LUMO}$ are the HOMO/LUMO orbital energies. According to Eq 4, the following two factors drive the conductance. First, is the alignment of frontier HOMO and LUMO orbitals w.r.t Fermi energy. The smaller HOMO-LUMO gap leads to smaller energy offset between the frontier MOs and Fermi level of the electrode, and results in higher conductance. Thus, a wire should possess a decreasing HOMO-LUMO gap with length. The second dominant factor is the numerator of Eq. 4, i.e., orbital coefficients at the contact sites which control the electrode–molecule coupling strength and should remain substantial with increasing length. Thus, the strong orbital localization at the contact sites and narrowing of HOMO-LUMO gap with length can commute an efficient electron transport with a plausible anti-ohmic behavior. Apart from these two factors, the delocalization of orbital over complete molecular backbone also provides an efficient conduction pathway and has been demonstrated to play a significant role in controlling the conductance.[66,67] A link between the electron delocalization patterns and the normal or reverse decay of conductance

with length was also established by Mandado et al.[68]

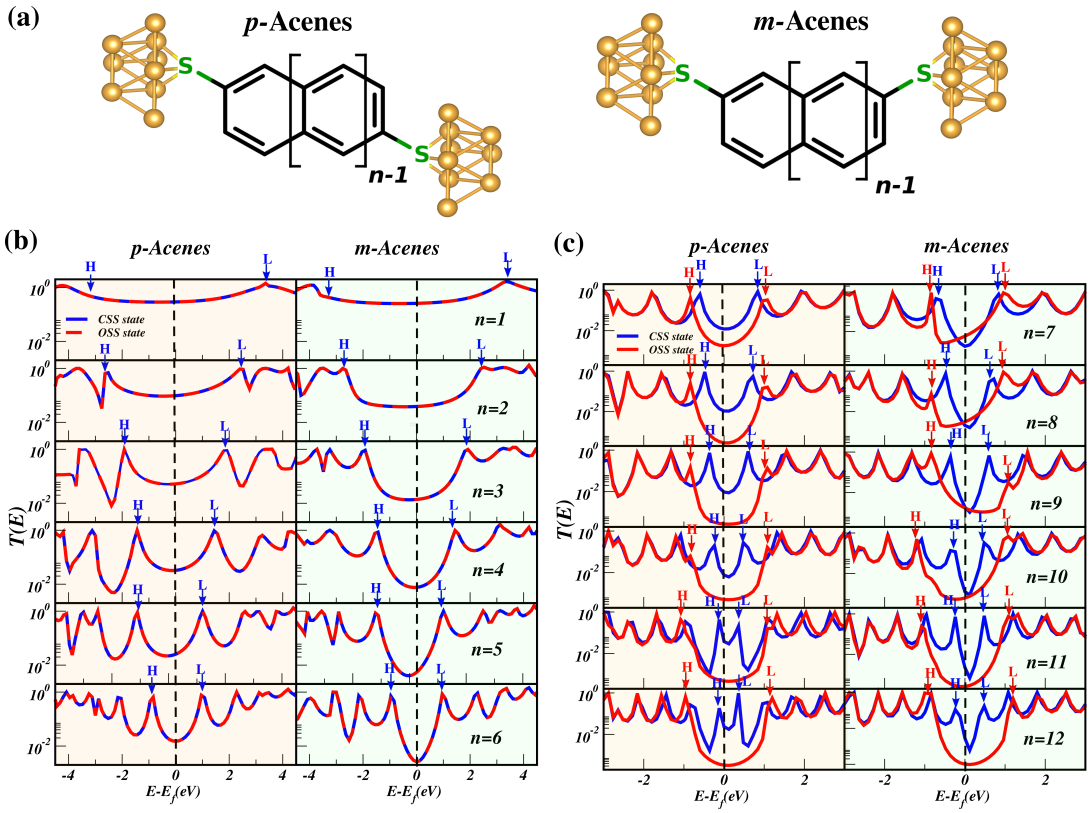


**Figure 2:** (a) Junction schematics showing para ($p$) and meta ($m$) connected acenes suspended between two $Au_9$ clusters via thiol anchoring groups. Calculated transmission spectra (b) for $n = 1$ to 6 $p$-acenes and $m$-acenes, (c) $n = 7$ to 12 $p$-acenes and $m$-acenes. The calculated transmission in CSS and OSS state is denoted by blue and red curves, respectively with blue/red arrows depicting frontier orbital energies in CSS/OSS state. The vertical dotted line denotes the position of Fermi level.

The transmission characteristics for $n = 1$ to 12 acenes in both CSS and OSS state is presented in Figure 2. As for polyacenes, we have previously reported that acenes with meta connection to electrodes lead to suppression of conductance as compared to their para connected analogs due to destructive quantum interference (DQI), which further intensify with increasing molecular length.[51] Thus, taking into consideration the fundamental role played by QI effects, we have examined acenes with both para and meta connections to Au electrodes (Figure 2a). Figure 2b shows the transmission spectra for $n = 1$ to 6 acenes in CSS state and OSS state, wherein the frontier orbital energies are marked with arrows. The evolution of transmission spectra and frontier orbital energies reveals several trends with

competing effects on conductance. The first is shifting of frontier orbital energies and the corresponding transmission peaks towards the Fermi energy with increase in $n$. Thereby, decreasing the energy gap between frontier peaks ($\varepsilon$) with increasing molecular length, which acts to increase the conductance. The second is the increase in number of resonant peaks appearing in conductance spectra with the increment of the length which also favours the increase in conductance. This is in line with the increase in density of MOs with increasing $n$, as illustrated in orbital energy diagram plot (Figure S9 in SI). The other competing factor is the broadening of the frontier resonant peaks ($\tau$), which results from the coupling of molecular states to the extended states of the electrode.[69] Although, the two factors, i.e., energy gap between frontier peaks ($\varepsilon$) and level broadening ($\tau$) associated with the strength of coupling are correlated to each other. Stronger the coupling between electrode and molecule, more the HOMO and LUMO resonance peaks move towards the Fermi energy and vice versa. However, for the described acene series, the two aforementioned factors play a contradictory role in controlling the conductance with increasing molecular length. With increasing $n$, the HOMO and LUMO resonances are moving closer to the Fermi energy, which is a consequence of the decrease of molecular HOMO-LUMO gap with the increasing length. Along with the HOMO-LUMO gap, the width of HOMO and LUMO resonances ($\tau$) also decreases simultaneously along the series. This can be directly inferred from the spatial distribution of MOs (Figure S3 in SI) which reveals that orbital coefficients falls off quickly at the terminal connecting sites with increasing length which eventually results in weak coupling with electrodes. The decrease in energy gap ($\varepsilon$) acts to increase the conductance, while the decrease in width of frontier peaks ($\tau$) acts to decrease the conductance. The interplay between $\varepsilon$ and $\tau$ was also used by Yelin et al.[70] to explain the conductance-length trends for acene series, wherein the conductance is described using a single-Lorentzian model : $G = G_0/[(\varepsilon/\tau)^2 + 1]$. With these competing factors, the conductance, determined by the magnitude of transmission coefficient at the Fermi energy, reveals an evident decrease with the increasing molecular length. All these trends including the decrease in conduc-

tance and evolution of frontier orbital energies are robust for both *p*-acenes and *m*-acenes. However, as compared to *p*-acenes, *m*-acenes shows sharp dips near Fermi energy owing to DQI effects associated with the phase difference between electron waves traversing across the molecule.[52,71,72] Noteworthy, since the electronic structure calculations in OSS state for $n = 1$ to 6 acenes converges to CSS ground state with $\Delta E_{OSS-CSS} = 0$ (Figure 1a), so does the transport calculations with identical transmission spectra and frontier orbital energies for closed shell and open shell calculations.

For higher acenes with OSS ground state, the transmission spectra for $n = 7$ to 12 in CSS and OSS ground state is shown in Figure 2c. In CSS state, the frontier transmission peaks near Fermi energy are shifted towards Fermi energy. Thereby, decreasing the energy gap with increasing $n$ to $\sim 0.70$ eV for $n$= 12 acene. But in OSS state, the frontier peaks are held in fixed positions, thus saturating the energy gap at $\sim 1.60$ eV from $n$= 7 to 12 acenes. This gap saturation is consistent with HOMO-LUMO gap for isolated acenes, which saturates to a constant value of $\sim 1.76$ eV in OSS state, but shows a steady decrease in CSS state (Figure S1 in SI). Similar gap stabilization for higher acenes was also reported by Pilevarshahri et al.[37] and Wilhelm et al. using GW-based methods.[73] Apart from the gap saturation, the other competing factors, i.e., number of resonant peaks and width of frontier resonant peaks also infuse to a constant value in OSS state. These saturation factors are accompanied by a significantly decreased transmission near Fermi level in OSS state as compared to CSS state which now appeared irrespective of para/meta configuration. For meta configuration, conductance shows an evident decrease up to $n = 12$, while for para configuration it saturates at $n = 8$. It is worth mentioning that CSS solution is indeed appropriate for smaller acenes with CSS ground state while for higher acenes with OSS ground state, the use of CSS solution is merely a computational artifact which leads to artificially enhanced transmission. Thus, the use of unrestricted solution for molecules bearing diradical character is mandatory for accurate estimation of conductance.

## 3.3 Validation for Cumulenes

To bring the observed contrasting features of transmission spectra in CSS and OSS state on more solid ground, we calculated the transmission spectra for another genre of molecular wires, i.e., cumulenes, shown in Figure 3. To simulate the experimental data, both the ends of cumulene molecules are substituted with phenyl groups, which enhance their stability.[45] The phenyl-substituted cumulenes are then placed between two $Au_9$ clusters using thiol linker atoms (Figure 3a). Interestingly, corroborated with previous theoretical[74] and experimental measurements,[43] cumulene wires provide us an example with desired anti-ohmic behavior. The comparison of computed conductance with experimentally reported values[43] from $C4$ to $C8$ (Table S14) reveals that B3LYP values overestimate the conductance by upto 2 orders of magnitude, while CAM-B3LYP yields conductance within 1 order of magnitude of the experimental values. Nonetheless, B3LYP produces a negative $\beta$ value of -0.136 which is in fair agreement with the experimental value of -0.120 from $C4$ to $C8$. The transmission characteristics for the lower members exhibiting CSS ground state (Figure 3b), indicates that the frontier transmission peaks approach towards Fermi energy with a decreasing energy gap in CSS state, while OSS converge to CSS with a slight variation for $C12$. For higher cumulenes in OSS ground state (Figure 3c), frontier resonance peaks in CSS state feature a contracting energy gap to 0.57 eV for $C24$, while transmission peaks in OSS state do evidence a gap saturation at $\sim$ 1.55 eV from $C14$ to $C24$ cumulenes. In addition to this, OSS state yields lower transmission peak heights than those of CSS state. This results in significantly decreased transmission near Fermi energy in OSS state as compared to CSS state. Notably, apart from the frontier transmission peaks residing near Fermi energy, all the transmission features away from the Fermi energy are nearly identical in CSS and OSS state, implying that spin symmetry breaking effects are negligible for those states.

It is now tempting to correlate the decay coefficients, $\beta$, in CSS and OSS state. Figure 4a shows the evolution of conductance as a function of $n$ for $p$-acenes and $m$-acenes. It outlines

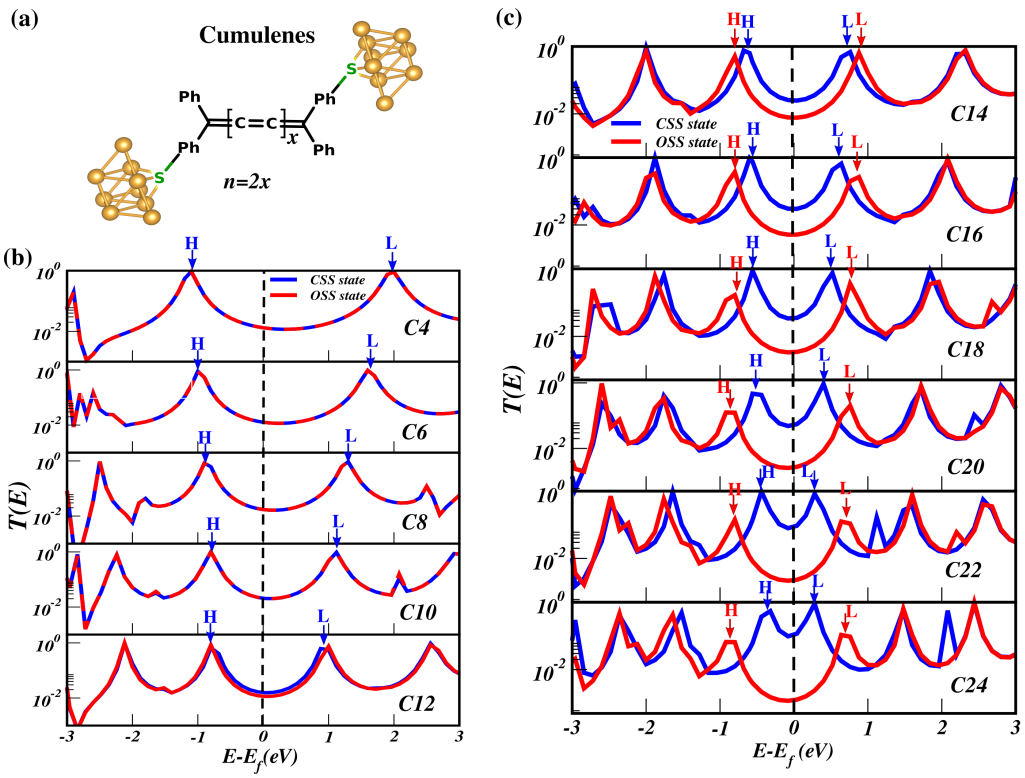


**Figure 3:** (a) Junction schematic showing phenyl-substituted cumulene ($C4$) suspended between two $Au_9$ clusters via thiol anchoring groups. Calculated transmission spectra as a function of energy for (b) lower cumulenes ($C4$ to $C14$), (c) for higher cumulenes ($C14$ to $C24$). The calculated transmission in CSS and OSS state is denoted by blue and red curves, respectively with blue/red arrows depicting frontier orbital energies in CSS/OSS state. The vertical dotted line denotes the position of Fermi level.

an overall trend of decreasing conductance with increasing molecular length, which is indeed unchanged in both CSS and OSS state. However, the decay is much steeper in OSS state than that in CSS state, as can be inferred from decay constant values, i.e. $\beta = 0.216$ in CSS state, whereas it increases to 0.768 in OSS state for $p$-acenes. Similarly, $m$-acenes yield $\beta = 0.312$ in CSS state and 0.563 in OSS state. This implies that in OSS state, longer molecules lead to even higher resistance. On contrary, for cumulenes (Figure 4b), inverted attenuation factors are observed. In CSS state, an increase in conductance is observed from $n = 4$ to 24 with negative $\beta$ value of 0.099. The origin of anti-ohmic behavior of cumulenes is rooted in to the frontier MOs (Figure S5 in SI) which are delocalized over the complete molecular backbone providing an efficient conducting pathway. More importantly, the delocalization of

MOs is further extended to the terminal connecting sites which facilitates strong electrode-molecule coupling. This is in contrast to polyacenes where orbital coefficients diminish quickly at the terminal benzene rings. The substantial weight of the conducting frontier MOs on the terminal contact sites together with decreasing HOMO-LUMO gap in cumulenes engender both the factors in Eq. 4 to favour an increase in conductance. However in OSS state, which is ground state for higher members, yields positive $\beta$ values of 0.134 with regular decay of conductance. Overall, the conductance increases upto a maximum wherein the lower members of the series with CSS ground state persist in anti-ohmic regime, in contrast, the emergence of OSS ground state for the higher members, provokes a regular decay of conductance. This indicates that anti-ohmic behavior do exists for lower cumulenes with CSS ground state, however if a restricted wavefunction is wrongly imposed to higher cumulenes with OSS ground state, it results in incorrect prediction of empirically negative $\beta$ values. A similar transformation from the length increasing conductance to normal decay of conductance was also oberved by Mandado et al. when BS-UKS-DFT was employed instead of RKS-DFT for a series of polymeric chains.[20] Thus, indicting that the suggested positive correlation between diradical character and conductance[18,75] is not as uni-equivocal.

To further understand the electronic structure governing the contrasting $\beta$ values in CSS and OSS state, the spatial distribution of frontier HOMO and LUMO orbitals and their energy gaps is shown in insets of Figure 4. The different behavior of electron transport in closed shell and broken-symmetry state was explained by Mandado et al. based on the spatial symmetry of frontier molecular spin orbitals.[20] Accordingly, in unrestricted broken symmetry ground state, a molecule is subjected to spin-symmetry breaking which produces different spin-split orbitals for $\alpha$ and $\beta$ electrons. As illustarted in Figure 4(a) for acenes, frontier orbitals are localized on both zig-zag sites of the central benzene rings in CSS state, while in OSS state, spin-split degenerate HOMOs, i.e., $\alpha$-HOMO is localized on the hydrogenated C-atoms at one edge of the molecule, while $\beta$-HOMO is localized on the other edge with a disjoint character. The spin-split degenerate LUMOs also reveal the similar

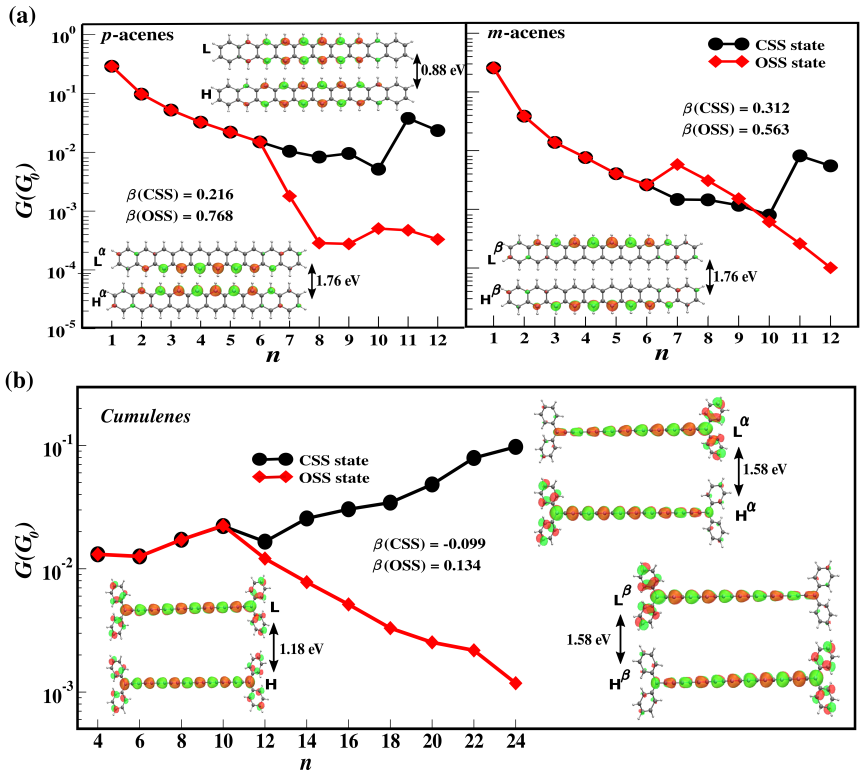


**Figure 4:** (a) Molecular conductance (in units of $G_0$) v/s number of benzene rings ($n$) in CSS state (black curve) and OSS state (red curve) for $p$-acenes and $m$-acenes. Both CSS and OSS state shows a regular decay of conductance along the series with large positive $\beta$ values in OSS state. (b) Conductance versus number of C-atoms ($n$) for phenyl-substituted cumulenes. CSS state yields a negative $\beta$ value with an increasing conductance, while OSS state reveals a decay of conductance for higher cumulene members. Spatial distribution of frontier HOMO and LUMO orbitals and HOMO-LUMO energy gaps are shown in insets for $n = 10$ acene and $n = 20$ cumulene.

disjoint character. Similarly, for cumulenes in OSS state, spin-symmetry breaking enforces the $\alpha$-HOMO and $\beta$-HOMO to localize at opposite ends, thereby decreasing the delocalized character of frontier MOs in OSS state. Apart from the symmetry breaking, OSS state witnesses a higher HOMO-LUMO gap as compared to CSS state (Figure S1 and S2 in SI). As discussed above, in CSS state the HOMO-LUMO gap approaches towards gap closure with the increasing length, while in OSS state, the gap is an exchange gap between the spin-split orbitals which is not strongly length dependent and saturates to a finite value. The decrease in delocalized nature of spin-split orbitals integrated with an increase of HOMO-LUMO gap in OSS state inhibits the efficient contact coupling in junction. This results in an

emphatic decrease in conductance with the increasing diradical character along the series.

## 3.4 Multi-configurational nature of Acenes

Besides this, when going to higher order polyacenes, the increasing near degeneracy of frontier orbitals (see Figure S9 and S10 in SI), induces strong electron correlation effects. Such molecular systems with high static correlations possess inherent multi-configurational character, which is well reflected from the $<S^2>_{BS}$ values (Table S5 in SI). The mean value of $S^2$ operator for the unrestricted $m_s = 0$ BS determinant should be 1.0, however $< S^2 >_{BS}$ values exceeding 1.0 from $n$ =8 onward indicates the contribution from the components of higher spin multiplicities and hence reflecting the multi-configurational character.[31,76] Moreover, the fractional occupation numbers of BS-UHF based natural orbitals (Table S7 of SI) used to compute the radicaloid character, reveals that the occupancy of frontier HONO and LUNO orbitals tends to approach one instead of two for $n$ >7 acenes.[63] Thus indicating the presence of two nearly singly occupied frontier orbitals and hence the open shell singlet character, which is well taken into account by the BS-UKS calculations. Apart from the HONO and LUNO, the similar trend is present to a lower degree for next nearest orbitals, i.e., HONO-1 and LUNO+1, with an increasing occupation number of LUNO+1 and a decreasing of that of HONO-1. For $n$ = 11, the occupation numbers of HONO-1 (1.29) and LUNO+1 (0.70) indeed support the idea of tetra-radical character, with four nearly singly occupied open shells. Nevertheless, the ground state remains open shell diradical in nature. In the context of increasing polyradical character for higher order acenes, a DMRG study by Chan et al. represent a deepest study of static correlations in acenes by performing a full $\pi$-valence space CASSCF calculations.[26] Within the DMRG formalism, this work also established singlet diradical ground state with the plausible evolution of polyradical ground state beyond $n$=12, which corroborates well with our predictions of BS-UKS DFT as well as previously reported by Malrieu et al.[31] More recently, Gagliardi et al. also presented the use of multiconfgurational pair density functional theory (MC-PDFT) to include the

dynamic electron correlations beyond that captured within a DMRG wavefunction, in a two-step procedure called DMRG-PDFT to compute the singlet-triplet gaps, however the study was rather limited to $n$=7 acenes.[77] Thus, although, multi-reference methods give better insights in to the electronic structure calculations of strongly correlated molecules. However, the electron transport through a molecular junction is pre-dominantly governed by spatial orientation of molecular orbitals acting as the conduction channels.[64] While, it does not matter whether the electronic states lying near the Fermi energy are filled, empty or partially occupied, as accurately predicted by multi-reference methods. On the other hand, individual orbital picture provided by DFT is more robust, which is a pre-requisite for transport calculations. Apart from the accurate orbital picture, BS-UKS method fairly describes the ground state open shell diradical configurations for lower order acenes.

# 4 Conclusion

In conclusion, the findings in this work add new prospective on the debate concerning the feasibility of anti-ohmic wires. The origin of anti-ohmic electron transport is rooted in to the intrinsic electronic structure of the molecule wherein the decreasing gap between frontier electronic states and its localization at the terminal connecting sites of junction drives a nanowire into anti-ohmic regime.[8,68] The current study put forth the preferential existence of the molecule in CSS state as another guiding rule to observe the desirable increase in conductance. We demonstrate that for acenes, decreasing orbital coefficients results in a regular decay of conductance in both CSS and OSS state, accompanied by a larger resistance in OSS state. On the other hand, cumulenes display a priori all of the features required to be a anti-ohmic wire. However, clouds over this horizon appear with the evolution from CSS to OSS state upon increasing length. For large enough molecules, the CSS state becomes unstable and undergoes spin-symmetry breaking which enforces $\alpha$ and $\beta$ electrons to localize at the opposite ends of the molecule. This dramatically reduces the delocalized nature of

frontier $\alpha/\beta$ channels yield a consequent decay of conductance as compared to their CSS counterparts. It is worth mentioning that CSS solution is indeed appropriate for lower members of the series with CSS ground state while it does not represent a physical state for higher order members with OSS ground state. The restricted CSS solutions results in enhanced transmission for higher members with incorrect prediction of small or even negative $\beta$ values. Thus, the use of unrestricted OSS solutions for molecules bearing diradical character is mandatory for accurate estimation of conductance. Overall, the findings in this work highlight that the inherent transition of intrinsic electronic structure from CSS to OSS ground state with increasing length enforces the molecule to yield a regular decay of conductance. Thus, emphasizing the existence of a molecule in closed-shell state along with the two pre-requisites of decreasing HOMO-LUMO gap and substantial orbital localization at connecting sites to observe the desired increase in conductance.

# Acknowledgement

Financial support from Department of Science and Technology through SERB-ECR project No. ECR/2016/000362 and SERB-CRG project No. CRG/2019/003237 is gratefully acknowledged.

**Supporting Information Available:** Computational details, computed total energies, $<S^2>$ values in gas phase and molecular junction, BS-UHF orbital occupancy, radicaloid character, HOMO-LUMO gap, spatial distribution and energetics of frontier MOs, spin density distribution, CAM-B3LYP computed conductance, odd cumulenes.

This material is available free of charge via the Internet at http:// pubs.acs.org.

# References

(1) Tao, N. J. Electron transport in molecular junctions. *Nanoscience And Technology: A Collection of Reviews from Nature Journals* **2010**, 185–193.

(2) Weiss, E. A.; Ahrens, M. J.; Sinks, L. E.; Gusev, A. V.; Ratner, M. A.; Wasielewski, M. R. Making a molecular wire: charge and spin transport through para-phenylene oligomers. *J. Am. Chem. Soc.* **2004**, *126*, 5577–5584.

(3) Ie, Y.; Okamoto, Y.; Inoue, T.; Tone, S.; Seo, T.; Honda, Y.; Tanaka, S.; Lee, S. K.; Ohto, T.; Yamada, R.; et al., Highly planar and completely insulated oligothiophenes: Effects of $\pi$-conjugation on hopping charge transport. *J. Phys. Chem. Lett.* **2019**, *10*, 3197–3204.

(4) Kolivoska, V.; Valaések, M.; Gál, M.; Sokolová, R.; Bulickova, J.; Pospisil, L.; Mészáros, G.; Hromadová, M. Single-molecule conductance in a series of extended viologen molecules. *J. Phys. Chem. Lett.* **2013**, *4*, 589–595.

(5) Lee, H. J.; Cho, S. J.; Kang, H.; He, X.; Yoon, H. J. Achieving ultralow, zero, and inverted tunneling attenuation coefficients in molecular wires with extended conjugation. *Small* **2021**, *17*, 2005711.

(6) Gunasekaran, S.; Hernangómez-Pérez, D.; Davydenko, I.; Marder, S.; Evers, F.; Venkataraman, L. Near length-independent conductance in polymethine molecular wires. *Nano Lett.* **2018**, *18*, 6387–6391.

(7) Kuang, G.; Chen, S.-Z.; Wang, W.; Lin, T.; Chen, K.; Shang, X.; Liu, P. N.; Lin, N. Resonant charge transport in conjugated molecular wires beyond 10 nm range. *J. Am. Chem. Soc.* **2016**, *138*, 11140–11143.

(8) Tada, T.; Yoshizawa, K. Reverse exponential decay of electrical transmission in nano-sized graphite sheets. *J. Phys. Chem. B* **2004**, *108*, 7565–7572.

(9) Li, Z.; Park, T.-H.; Rawson, J.; Therien, M. J.; Borguet, E. Quasi-ohmic single molecule charge transport through highly conjugated meso-to-meso ethyne-bridged porphyrin wires. *Nano Lett.* **2012**, *12*, 2722–2727.

(10) Sedghi, G.; García-Suárez, V. M.; Esdaile, L. J.; Anderson, H. L.; Lambert, C. J.; Martín, S.; Bethell, D.; Higgins, S. J.; Elliott, M.; Bennett, N.; et al., Long-range electron tunnelling in oligo-porphyrin molecular wires. *Nat. Nanotechnol.* **2011**, *6*, 517–523.

(11) Leary, E.; Limburg, B.; Alanazy, A.; Sangtarash, S.; Grace, I.; Swada, K.; Esdaile, L. J.; Noori, M.; González, M. T.; Rubio-Bollinger, G.; et al., Bias-driven conductance increase with length in porphyrin tapes. *J. Am. Chem. Soc.* **2018**, *140*, 12877–12883.

(12) Tsuji, Y.; Movassagh, R.; Datta, S.; Hoffmann, R. Exponential attenuation of through-bond transmission in a polyene: Theory and potential realizations. *ACS nano* **2015**, *9*, 11109–11120.

(13) Ramos-Berdullas, N.; Mandado, M. Electronic properties of p-xylylene and p-phenylene chains subjected to finite bias voltages: A new highly conducting oligophenyl structure. *Chem. Eur. J.* **2013**, *19*, 3646–3654.

(14) Stuyver, T.; Zeng, T.; Tsuji, Y.; Fias, S.; Geerlings, P.; De Proft, F. Captodative substitution: a strategy for enhancing the conductivity of molecular electronic devices. *J. Phys. Chem. C* **2018**, *122*, 3194–3200.

(15) Gil-Guerrero, S.; Ramos-Berdullas, N.; Mandado, M. Can aromaticity enhance the electron transport in molecular wires? *Org. Electron.* **2018**, *61*, 177–184.

(16) Li, L.; Low, J. Z.; Wilhelm, J.; Liao, G.; Gunasekaran, S.; Prindle, C. R.; Starr, R. L.; Golze, D.; Nuckolls, C.; Steigerwald, M. L.; et al., Highly conducting single-molecule topological insulators based on mono-and di-radical cations. *Nat. Chem.* **2022**, 1–7.

(17) Stuyver, T.; Fias, S.; De Proft, F.; Geerlings, P.; Tsuji, Y.; Hoffmann, R. Enhancing the conductivity of molecular electronic devices. *J. Chem. Phys.* **2017**, *146*, 092310.

(18) Stuyver, T.; Zeng, T.; Tsuji, Y.; Geerlings, P.; De Proft, F. Diradical character as a guiding principle for the insightful design of molecular nanowires with an increasing conductance with length. *Nano Lett.* **2018**, *18*, 7298–7304.

(19) Gil-Guerrero, S.; Peña-Gallego, Á.; Ramos-Berdullas, N.; Martin Pendas, A.; Mandado, M. Assessing the reversed exponential decay of the electrical conductance in molecular wires: the undeniable effect of static electron correlation. *Nano Lett.* **2019**, *19*, 7394–7399.

(20) Ramos-Berdullas, N.; Gil-Guerrero, S.; Peña-Gallego, Á.; Mandado, M. The effect of spin polarization on the electron transport of molecular wires with diradical character. *Phys. Chem. Chem. Phys.* **2021**, *23*, 4777–4783.

(21) Houk, K.; Lee, P. S.; Nendel, M. Polyacene and cyclacene geometries and electronic structures: bond equalization, vanishing band gaps, and triplet ground states contrast with polyacetylene. *J. Org. Chem.* **2001**, *66*, 5517–5521.

(22) Dos Santos, M. Electronic properties of acenes: Oligomer to polymer structure. *Phys. Rev. B* **2006**, *74*, 045426.

(23) Bendikov, M.; Duong, H. M.; Starkey, K.; Houk, K.; Carter, E. A.; Wudl, F. Oligoacenes: theoretical prediction of open-shell singlet diradical ground states. *J. Am. Chem. Soc.* **2004**, *126*, 7416–7417.

(24) Mondal, R.; Tonshoff, C.; Khon, D.; Neckers, D. C.; Bettinger, H. F. Synthesis, stability, and photochemistry of pentacene, hexacene, and heptacene: A matrix isolation study. *J. Am. Chem. Soc.* **2009**, *131*, 14281–14289.

(25) Zuzak, R.; Dorel, R.; Krawiec, M.; Such, B.; Kolmer, M.; Szymonski, M.; Echavarren, A. M.; Godlewski, S. Nonacene generated by on-surface dehydrogenation. *ACS nano* **2017**, *11*, 9321–9329.

(26) Hachmann, J.; Dorando, J. J.; Avilés, M.; Chan, G. K.-L. The radical character of the acenes: A density matrix renormalization group study. *J. Chem. Phys.* **2007**, *127*, 134309.

(27) Jiang, D.-e.; Dai, S. Electronic ground state of higher acenes. *J. Phys. Chem. A* **2008**, *112*, 332–335.

(28) Hajgató, B.; Huzak, M.; Deleuze, M. S. Focal point analysis of the singlet–triplet energy gap of octacene and larger acenes. *J. Phys. Chem. A* **2011**, *115*, 9282–9293.

(29) Yang, Y.; Davidson, E. R.; Yang, W. Nature of ground and electronic excited states of higher acenes. *Proc. Natl. Acad. Sci.* **2016**, *113*, E5098–E5107.

(30) Dupuy, N.; Casula, M. Fate of the open-shell singlet ground state in the experimentally accessible acenes: A quantum Monte Carlo study. *J. Chem. Phys.* **2018**, *148*, 134112.

(31) Trinquier, G.; David, G.; Malrieu, J.-P. Qualitative views on the polyradical character of long acenes. *J. Phys. Chem. A* **2018**, *122*, 6926–6933.

(32) Maiti, S. K. Quantum transport through polycyclic hydrocarbon molecules. *Phys. Lett. A* **2007**, *366*, 114–119.

(33) Zhou, Y.; Jiang, F.; Chen, H.; Note, R.; Mizuseki, H.; Kawazoe, Y. Quantum length dependence of conductance in oligomers: First-principles calculations. *Phys. Rev. B* **2007**, *75*, 245407.

(34) Liu, H.; Ni, W.; Zhao, J.; Wang, N.; Guo, Y.; Taketsugu, T.; Kiguchi, M.; Murakoshi, K. Nonequilibrium Green's function study on the electronic structure and transportation behavior of the conjugated molecular junction: Terminal connections and intramolecular connections. *J. Chem. Phys.* **2009**, *130*, 244501.

(35) He, Y.; Cheng, N.; Zhao, J. First-principle study on the conductance of benzene-based

molecules with various bonding characteristics. *Comput. Theor. Chem.* **2019**, *1154*, 1–10.

(36) Gryn'ova, G.; Corminboeuf, C. Topology-driven single-molecule conductance of carbon nanothreads. *J. Phys. Chem. Lett.* **2019**, *10*, 825–830.

(37) Pilevarshahri, R.; Rungger, I.; Archer, T.; Sanvito, S.; Shahtahmassebi, N. Spin transport in higher n-acene molecules. *Phys. Rev. B* **2011**, *84*, 174437.

(38) Visontai, D.; Grace, I.; Lambert, C. Electron transport through ribbonlike molecular wires calculated using density-functional theory and Green's function formalism. *Phys. Rev. B* **2010**, *81*, 035409.

(39) Kaliginedi, V.; Moreno-García, P.; Valkenier, H.; Hong, W.; García-Suárez, V. M.; Buiter, P.; Otten, J. L.; Hummelen, J. C.; Lambert, C. J.; Wandlowski, T. Correlations between molecular structure and single-junction conductance: a case study with oligo (phenylene-ethynylene)-type wires. *J. Am. Chem. Soc.* **2012**, *134*, 5262–5275.

(40) Valdiviezo, J.; Rocha, P.; Polakovsky, A.; Palma, J. L. Nonexponential Length Dependence of Molecular Conductance in Acene-Based Molecular Wires. *ACS sensors* **2021**, *6*, 477–484.

(41) Wang, C.; Batsanov, A. S.; Bryce, M. R.; Martin, S.; Nichols, R. J.; Higgins, S. J.; Garcia-Suarez, V. M.; Lambert, C. J. Oligoyne single molecule wires. *J. Am. Chem. Soc.* **2009**, *131*, 15647–15654.

(42) Jasper-Tönnies, T.; Garcia-Lekue, A.; Frederiksen, T.; Ulrich, S.; Herges, R.; Berndt, R. Conductance of a freestanding conjugated molecular wire. *Phys. Rev. Lett.* **2017**, *119*, 066801.

(43) Zang, Y.; Fu, T.; Zou, Q.; Ng, F.; Li, H.; Steigerwald, M. L.; Nuckolls, C.; Venkatara-

man, L. Cumulene wires display increasing conductance with increasing length. *Nano Lett.* **2020**, *20*, 8415–8419.

(44) Xu, W.; Leary, E.; Hou, S.; Sangtarash, S.; González, M. T.; Rubio-Bollinger, G.; Wu, Q.; Sadeghi, H.; Tejerina, L.; Christensen, K. E.; et al., Unusual length dependence of the conductance in cumulene molecular wires. *Angew. Chem. Int. Ed.* **2019**, *131*, 8466–8470.

(45) Wendinger, D.; Tykwinski, R. R. Odd [n] cumulenes (n= 3, 5, 7, 9): synthesis, characterization, and reactivity. *Acc. Chem. Res.* **2017**, *50*, 1468–1479.

(46) Januszewski, J. A.; Wendinger, D.; Methfessel, C. D.; Hampel, F.; Tykwinski, R. R. Synthesis and structure of tetraarylcumulenes: Characterization of bond-length alternation versus molecule length. *Angew. Chem. Int. Ed.* **2013**, *52*, 1817–1821.

(47) Beck, A. D. Density-functional thermochemistry. III. The role of exact exchange. *J. Chem. Phys* **1993**, *98*, 5648–6.

(48) Weigend, F.; Ahlrichs, R. Balanced basis sets of split valence, triple zeta valence and quadruple zeta valence quality for H to Rn: Design and assessment of accuracy. *Phys. Chem. Chem. Phys.* **2005**, *7*, 3297–3305.

(49) Neese, F. The ORCA program system. *Wiley Interdiscip. Rev. Comput. Mol. Sci.* **2012**, *2*, 73–78.

(50) Neese, F.; Wennmohs, F.; Hansen, A.; Becker, U. Efficient, approximate and parallel Hartree–Fock and hybrid DFT calculations. A chain-of-spheres algorithm for the Hartree–Fock exchange. *Chem. Phys.* **2009**, *356*, 98–109.

(51) Bajaj, A.; Kaur, P.; Sud, A.; Berritta, M.; Ali, M. E. Anomalous effect of quantum interference in organic spin filters. *J. Phys. Chem. C .* **2020**, *124*, 24361–24371.

(52) Bajaj, A.; Khurana, R.; Ali, M. E. Quantum interference and spin filtering effects in photo-responsive single molecule devices. *J. Mater. Chem. C* **2021**, *9*, 11242 – 11251.

(53) Deffner, M.; Groß, L.; Steenbock, T.; Voigt, B.; Solomon, G.; Herrmann, C. Artaios—a code for postprocessing quantum chemical electronic structure calculations. 2010.

(54) Pastawski, H. M. Classical and quantum transport from generalized Landauer-Büttiker equations. *Phys. Rev. B* **1991**, *44*, 6329.

(55) Herrmann, C.; Solomon, G. C.; Subotnik, J. E.; Mujica, V.; Ratner, M. A. Ghost transmission: How large basis sets can make electron transport calculations worse. *J. Chem. Phys.* **2010**, *132*, 024103.

(56) Herrmann, C.; Solomon, G. C.; Ratner, M. A. Designing organic spin filters in the coherent tunneling regime. *J. Chem. Phys.* **2011**, *134*, 224306.

(57) Stein, T.; Eisenberg, H.; Kronik, L.; Baer, R. Fundamental gaps in finite systems from eigenvalues of a generalized Kohn-Sham method. *Phys. Rev. Lett.* **2010**, *105*, 266802.

(58) Refaely-Abramson, S.; Baer, R.; Kronik, L. Fundamental and excitation gaps in molecules of relevance for organic photovoltaics from an optimally tuned range-separated hybrid functional. *Phys. Rev. B* **2011**, *84*, 075144.

(59) Yamada, A.; Feng, Q.; Hoskins, A.; Fenk, K. D.; Dunietz, B. D. Achieving predictive description of molecular conductance by using a range-separated hybrid functional. *Nano Lett.* **2016**, *16*, 6092–6098.

(60) Bhandari, S.; Yamada, A.; Hoskins, A.; Payne, J.; Aksu, H.; Dunietz, B. D. Achieving predictive description of negative differential resistance in molecular junctions using a range-separated hybrid functional. *Adv. Theory Simul.* **2021**, *4*, 2000016.

(61) Khurana, R.; Bajaj, A.; Ali, M. E. Tuning the magnetic properties of a diamagnetic di-Blatter's zwitterion to antiferro-and ferromagnetically coupled diradicals. *Phys. Chem. Chem. Phys.* **2022**, *24*, 2543–2553.

(62) Kaur, P.; Ali, M. E. First principle investigations of long-range magnetic exchange interactions via polyacene coupler. *Int. J. Quantum Chem.* **2021**, DOI: https://doi.org/10.1002/qua.26756.

(63) Yamaguchi, K. The electronic structures of biradicals in the unrestricted Hartree-Fock approximation. *Chem. Phys. Lett.* **1975**, *33*, 330–335.

(64) Yoshizawa, K.; Tada, T.; Staykov, A. Orbital views of the electron transport in molecular devices. *J. Am. Chem. Soc.* **2008**, *130*, 9406–9413.

(65) Caroli, C.; Combescot, R.; Nozieres, P.; Saint-James, D. Direct calculation of the tunneling current. *J. Phys. C: Solid St. Phys.* **1971**, *4*, 916.

(66) Derosa, P. A.; Seminario, J. M. Electron transport through single molecules: Scattering treatment using density functional and green function theories. *J. Phys. Chem. B* **2001**, *105*, 471–481.

(67) Heurich, J.; Cuevas, J.; Wenzel, W.; Schön, G. Electrical transport through single-molecule junctions: from molecular orbitals to conduction channels. *Phys. Rev. Lett.* **2002**, *88*, 256803.

(68) Gil-Guerrero, S.; Ramos-Berdullas, N.; Pendás, Á. M.; Francisco, E.; Mandado, M. Anti-ohmic single molecule electron transport: is it feasible? *Nanoscale Adv.* **2019**, *1*, 1901–1913.

(69) Moth-Poulsen, K.; Bjørnholm, T. Molecular electronics with single molecules in solid-state devices. *Nat. Nanotechnol.* **2009**, *4*, 551–556.

(70) Yelin, T.; Korytár, R.; Sukenik, N.; Vardimon, R.; Kumar, B.; Nuckolls, C.; Evers, F.; Tal, O. Conductance saturation in a series of highly transmitting molecular junctions. *Nat. Mater. 15*, 444–449.

(71) Aggarwal, A.; Kaliginedi, V.; Maiti, P. K. Quantum circuit rules for molecular electronic systems: Where are we headed based on the current understanding of quantum interference, thermoelectric, and molecular spintronics phenomena? *Nano Lett.* **2021**, *21*, 8532–8544.

(72) Soni, S.; Ye, G.; Zheng, J.; Zhang, Y.; Asyuda, A.; Zharnikov, M.; Hong, W.; Chiechi, R. C. Understanding the Role of Parallel Pathways via In-Situ Switching of Quantum Interference in Molecular Tunneling Junctions. *Angew. Chem. Int. Ed.* **2020**, *59*, 14308–14312.

(73) Wilhelm, J.; Del Ben, M.; Hutter, J. GW in the Gaussian and plane waves scheme with application to linear acenes. *J. Chem. Theory Comput* **2016**, *12*, 3623–3635.

(74) Garner, M. H.; Bro-Jørgensen, W.; Pedersen, P. D.; Solomon, G. C. Reverse bond-length alternation in cumulenes: Candidates for increasing electronic transmission with length. *J. Phys. Chem. C* **2018**, *122*, 26777–26789.

(75) Tsuji, Y.; Okazawa, K.; Chen, B.; Yoshizawa, K. Mechanical control of molecular conductance and diradical character in bond stretching and $\pi$-stack compression. *J. Phys. Chem. C* . **2020**, *124*, 22941–22958.

(76) Kaur, P.; Ali, M. E. Influence of the radicaloid character of polyaromatic hydrocarbon couplers on magnetic exchange interactions. *ChemRxiv* **2021**, doi: `https://doi.org/10.26434/chemrxiv.14527185.v1`.

(77) Sharma, P.; Bernales, V.; Knecht, S.; Truhlar, D. G.; Gagliardi, L. Density matrix renormalization group pair-density functional theory (DMRG-PDFT): singlet–triplet gaps in polyacenes and polyacetylenes. *Chem. Sci.* **2019**, *10*, 1716–1723.

# Graphical TOC Entry